Letter

Phase diagram detection via Gaussian fitting of number probability distribution

Daniele Contessi [1,2,3,*] Alessio Recati [1,†] and Matteo Rizzi [2,3,‡]

[1] *Dipartimento di Fisica, Università di Trento and INO-CNR BEC Center, 38123 Povo, Italy*

[2] *Forschungszentrum Jülich GmbH, Institute of Quantum Control, Peter Grünberg Institut (PGI-8), 52425 Jülich, Germany*

[3] *Institute for Theoretical Physics, University of Cologne, D-50937 Köln, Germany*

(Received 19 July 2022; revised 2 February 2023; accepted 6 February 2023; published 10 March 2023)

We investigate the number probability density function that characterizes subportions of a quantum many-body system with globally conserved number of particles. We put forward a linear fitting protocol capable of mapping out the ground-state phase diagram of the rich one-dimensional extended Bose-Hubbard model: The results are quantitatively comparable with more sophisticated traditional and machine learning techniques. We argue that the studied quantity should be considered among the most informative bipartite properties, being moreover readily accessible in atomic gases experiments.

DOI: 10.1103/PhysRevB.107.L121403

I. INTRODUCTION

In recent years, quantum information and condensed matter theory have considerably cross fertilized, and a wealth of properties (mainly) of bipartite systems have emerged as powerful indicators of the many-body wave-function properties. With their help, quantum phases of matter and transitions between them have been characterized, and put in relation with the underlying quantum field theories. When dealing with the reduced density matrix of a subsystem, concepts like the entropy of the associated probability distribution, as well as its spectrum (technically the Schmidt singular values), are indeed unveiling the entanglement properties of the state of the system. A first prominent example is the logarithm scaling of the von Neumann (and, more generally, of any Rényi) entanglement entropy with the bipartition size for one-dimensional critical systems with local Hamiltonians [1–3]: Fitting the coefficient in front of such law is arguably one of the best ways to estimate the so-called central charge c of the associated conformal field theory (CFT). As a counterpart, the entanglement spectrum (ES) itself has been proven to exhibit peculiar properties both in gapless and gapped phases [4–6], and its degeneracy pattern is often used to tell different kinds of topological phases apart [7,8]. Its structures embed information about nonlocal quantum correlations, as formalized within the bulk-boundary correspondence framework [9–11]. Both *ad hoc* defined order parameters [12,13] and machine learning driven approaches [14–16] have been employed for the detection of phase transitions. Last, but certainly not least, the evolution of entanglement properties under the system dynamics has recently unveiled the existence of new kinds of nonequilibrium phase transitions for quantum many-body systems under random projective measurements or unitary gates [17–19].

As a consequence of the above, considerable efforts have been spent towards making such entanglement features measurable in the laboratory [20–24]. Among the many, the so-called number entanglement entropy is gaining a prominent role: Its operational definition refers to the probability density function (PDF) of a U(1) globally conserved charge in an extensive subportion of the system, also for mixed states [25]. Evidences of its distinctive dynamical behavior as a hallmark for many-body localization have been recently obtained numerically and experimentally [26–28].

A specific property of the PDF has been explored in the past, namely, its second momentum or, in other words, the amount of charge fluctuations $\mathcal{F}$ across subsystems. As very extensively explained in [29], a lot of properties of the fluctuations are shared with the entanglement entropy: for a gapped phase, they exhibit a strict area-law behavior, $\mathcal{F} \propto L^{d-1}$, with L the linear size of the partition and d the dimension of the system, whereas for a gapless phase there appears a logarithmic correction: $\mathcal{F} \propto L^{d-1} \ln L$ [30]. In particular, for a Luttinger liquid, the scaling coefficient is related to the K parameter, thus yielding yet another piece of information about the underlying field theory.

In this Letter, we propose an approach to map out the phase diagram of quantum many-body systems by considering the full PDF. We are able to detect all the phase transitions of the one-dimensional extended Bose-Hubbard (EBH) model at zero temperature by performing a simple and yet very general procedure consisting of some educated fits of the PDF only, therefore without resorting to any phase-specific quantity such as order parameter or correlation. We show how the PDF, being intimately related with the ES, preserves its intrinsic wealth of information about the nature of the phases. This can be exploited for an agnostic and automatic detection, as done with the machine learning solutions to the problem involving the ES. The huge advantage of the full PDF is its availability in experiments, e.g., with quantum gas microscopes, and not only in numerical simulations like the ones we perform here via matrix-product-states (MPS) simulations with embedded

*daniele.contessi@unitn.it
†alessio.recati@unitn.it
‡m.rizzi@fz-juelich.de

quantum numbers. We also show that a finite-size scaling analysis of the PDF leads to a pretty precise determination of the phase boundaries, and that some previously found functional forms of the PDF for limiting scenarios [3,31–35] can be connected to each other.

II. MODEL AND METHOD

The Hamiltonian of the one-dimensional EBH model can be written as

$$H = \sum_{j=1}^{L} \left(-t(b_{j+1}^{\dagger} b_j + \text{H.c.}) + \frac{U}{2} n_j(n_j - 1) + V n_j n_{j+1} \right), \tag{1}$$

where $b_j^{(\dagger)}$ is the annihilation (creation) bosonic operator and $n_j = b_j^{\dagger} b_j$ the number operator on site j along a one-dimensional chain with periodic boundary conditions (PBCs). The hopping coefficient is denoted by t, while U and V are the on-site and nearest-neighbor interaction strengths. The zero-temperature phase diagram of the unitary integer filled lattice, $\nu = N/L = 1$, presents a number of prototypical quantum phase transitions [36,37]: (i) a Berezinskii-Kosterlitz-Thouless (BKT) transition between a gapless superfluid (SF) and a gapped Mott insulator (MI) phase, (ii) a $c = 1$ transition between the MI and a topological Haldane insulator (HI), and (iii) an Ising $c = 1/2$ transition between the HI and a charge density-wave (CDW) state. Moreover, it has been recently pointed out that a phase-separated regime between SF and supersolid (SF + SS) [15,38] is present in the bottom right corner of the phase diagram. We set the energy scale by taking $t = 1$, and focus on the region $U \in [0, 6]$ and $V \in [0, 5]$ in order to have a direct comparison with the works in [15,36].

We determine the ground state $|\psi_g\rangle$ of the EBH model for various parameters by means of a MPS ansatz with U(1) symmetric tensors. Indeed the EBH model is nonintegrable and our numerical treatment is an almost unbiased approach to it. We set the maximum occupation to $n_{\max} = 4$ bosons per site. We deal with PBCs by employing a loop-free geometry of the tensor network and shifting the topology of the lattice into the matrix product operator (MPO) representation of the Hamiltonian (see the Supplemental Material of [39] for a detailed description). In this way, we can reliably compute relevant quantities for systems up to $L = 256$ sites, with a discarded probability not exceeding 10^{-9}.

We consider the system as divided into two equal portions A and $\bar{A}$: While the total number of particles is conserved, the number in the single region can fluctuate. The measurement of a deviation $\delta n = m$ from the average density happens with a probability

$$p(\delta n = m) = \text{Tr}(\rho_A \Pi_{N/2+m}) = \sum_{\alpha} \lambda_{\alpha}^{(m)}, \tag{2}$$

where $\rho_A := \text{Tr}_{\bar{A}} |\psi_g\rangle\langle\psi_g|$ is the reduced density matrix of subsystem A, and $\Pi_{N/2+m}$ is the projector on the sector with $N/2 + m$ occupancy. In the last equality we introduced the eigenvalues $\lambda_{\alpha}^{(m)}$ of ρ_A in the $N_A = N/2 + m$ particles sector: They are also related to so-called ES eigenvalues $\xi_{\alpha}^{(m)}$, via the relation $\lambda_{\alpha}^{(m)} = e^{-\xi_{\alpha}^{(m)}}$ [7,8]. Being the $\lambda_{\alpha}^{(m)}$'s the natural metric on which truncations of the tensor network representation are performed, the PDF is automatically at disposal without extra computational costs. We notice here that, in an experimental setup with access to site-resolved populations, the PDF is obtained by bin counting the occupation numbers in half of the system [26].

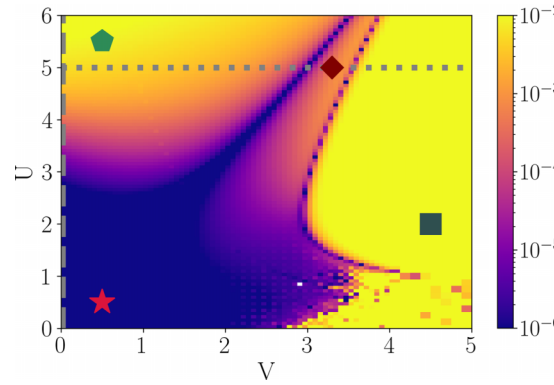

FIG. 1. Phase diagram of the EBH model traced with the residuals of the PDF's quadratic fit $p(m) \propto e^{-\beta m^2}$ for a $L = 64$ system. Details about the phase transitions along the dashed and dotted cuts are shown in Fig. 2. The PDFs correspondent to the configurations marked with the colored shapes are displayed below in Fig. 3.

III. GAUSSIAN FIT OF THE DENSITY PDF

For gapless one-dimensional phases described by a CFT, the PDF is a Gaussian, $p(m) \propto \exp(-\beta m^2)$, due to the presence of a single bosonic generator in the theory [29,32,40]. More precisely, the ES has been shown to be organized in equally spaced parabolas $\xi_{\alpha\equiv(k,\gamma)}^{(m)} = \xi_0 + k\xi_1 + \beta m^2$, where the index $\alpha = (k, \gamma)$ denotes the order of the parabola and the degeneracy of the eigenvalue, respectively, ξ_0 is the lowest eigenvalue of the ES, and ξ_1 the difference between the lowest and the second eigenvalue in the $m = 0$ particle sector [5]. As we will detail below, we expect instead the PDF of gapped phases to exhibit sensible deviations from this picture [6].

From the operational perspective, the differences between Gaussian and other PDF profiles can be captured via the average residuals of a two-parameter linear fit, namely, $1/N_m \sum_m [\ln p(m) + \beta m^2 + \beta']^2$ with N_m the number of fitted points and β' a normalization-related parameter. In Fig. 1 we plot (the logarithm of) such quantity over the span $m \in [-4, 4]$ for a fit performed upon the distribution values for $m \in [-2, 2]$. This simple procedure turns out to be very effective to map out the entire phase diagram even without prior knowledge of the phases and the PDF shapes to be expected. We find perfect agreement with previous studies [15,36], without resorting to any study of the correlation functions or gap nor to the use of machine learning techniques and, even more importantly, by using an experimentally very accessible quantity. For the interested reader, we also provide in [41] the same Fig. 1 computed from data of the simulated state-of-the-art experiments in which we reconstruct the PDF and we fit it from snapshots of the system for the particle counting. The results show that with a feasible number of snapshots, it is in principle possible to achieve a resolution comparable to the numerical study.

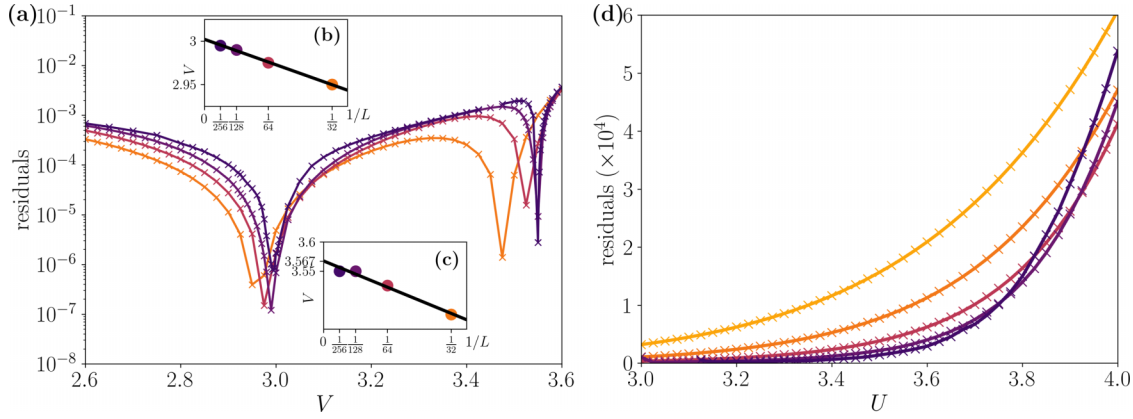

FIG. 2. Residuals of a Gaussian fit of the PDF $p(m) \propto e^{-\beta m^2}$ for different system's sizes $L = 16, 32, 64, 128, 256$ from light to dark color in the proximity of (a) the gapped-to-gapped phase transitions MI-HI-CDW along the cut $U = 5$ and (d) the gapless-to-gapped phase transitions SF-MI (BKT) for $V = 0$. In the insets, the location of the residuals' minimum is fitted against the inverse of the system's size in order to extrapolate the critical V_C for the MI-HI phase transition (b) and the HI-CDW transition (c).

It is worth noticing that our method properly identifies even the recently postulated SF + SS phase, which appears as a very noisy region in Fig. 1. This is a consequence of the alternation of uniform density regions and density-wave ordered ones [38]: The PDF is peaked on a value which is not necessarily the average density but depends on the location of the supersolid domains [41]. Since the PBC let this domain emerge in random positions along the ring, this gives rise to the above-mentioned noise.

Moreover, the nature of the phase transitions is reflected in the evolution of the residuals in their vicinity: In Fig. 2 we show the trend of the average residuals for two cuts of the phase diagram and different system's sizes ($L = 16, 32, 64, 128, 256$ from light to dark color). The first cut of Fig. 2(a) contains two gapped-to-gapped phase transitions for fixed $U = 5$, from MI to HI and from HI to CDW as indicated with a dotted line in Fig. 1. The location of the critical points is easily determined by the abrupt decrease of the residuals which becomes sharper and sharper as the length of the ring increases: In the two insets Figs. 2(b) and 2(c) a detail on the scaling of the critical V_C against the inverse of the system size is shown together with a linear fit. The extrapolation of the critical values is in perfect agreement with the previous studies, i.e., $V = 2.95 \pm 0.05$ for the transition MI-HI and $V = 3.525 \pm 0.05$ for HI-CDW [36].

The second cut Fig. 2(d) encompasses the gapless-to-gapped BKT phase transition from the SF to the MI at $V = 0$, indicated as a vertical dashed line in Fig. 1. It would be interesting to find a scaling procedure for the residuals, similarly to what is performed for the superfluid stiffness and/or the K-Luttinger parameter in standard approaches: At the moment, this remains, however, an open problem. We stress, however, that the β parameter of the linear fit offers a direct experimental access to the K-Luttinger parameter [29]. For completeness, we perform such an analysis in [41] (see, also, Refs. [42,43] therein) and we obtain a critical value $U_c \simeq 3.36 \pm 0.01$ in perfect agreement with previous studies as reported in [44]. The location of the transition corresponds to the uprising of the residuals.

IV. SHIFTED GAUSSIAN PDF FOR GAPPED PHASES

A more detailed look at the PDF unveils actually more information than the simple residuals to Gaussian fitting discussed above. In Fig. 3 we present some prototypical configurations in the different phases, corresponding to the colored symbols in the phase diagram of Fig. 1: e.g., panel (a) shows the perfect parabola for the SF phase. The striking feature is that all PDF profiles can be captured by proper shifts and combination of Gaussian envelopes, as we explain here below.

The shape of the PDF deep in the gapped phases can be computed resorting to boundary-linked perturbation theory [6]. For example, the ES levels for the MI are obtained by consecutive applications of the kinetic term $H' = \sum_{j=1}^{L} -t(b_{j+1}^{\dagger} b_j + \text{H.c.})$ on the zero-order ground state, i.e., $|\ldots 111 \ldots\rangle$. We are then interested primarily in achieving a given unbalance m with the minimal number of moves (i.e., perturbative orders of H'). In the case of a single boundary, it is rather easy to see that the leading order amounts to $(t/U)^{|m|(|m|+1)/2}$, up to a global weight depending on the ratio between the accumulated bosonic factors and the excitation energies along all possible sequences of moves [41]. When dealing with two boundaries, simple combinatorics leads to $p(m) \simeq \ln(t/U)^{\lfloor \frac{(|m|+1)^2}{4} \rfloor}$. The expression describes a symmetric envelope around the average number of particles, which could be recovered also by considering two symmetrical Gaussians shifted by ∓ 1 with respect to $m = 0$, for the positive and negative values of m, respectively. Remarkably, we find such horizontally shifted envelopes to persist with reduced offset when approaching the critical point, finally merging back when transitioning to the superfluid phase [see Figs. 3(b)–3(e)]. We also highlight here that a similar shift is the dominating feature of the PDF for the CDW phase, this time tending to ± 2 deep in the perturbative regime, hinting at the underlying structure of the zero-order ground state, i.e., $|\ldots 0202 \ldots\rangle$ [see Figs. 3(c)–3(f)].

The appearance of the $|m|$ dependence in the exponent due to a nonzero shift of these double parabolic envelopes

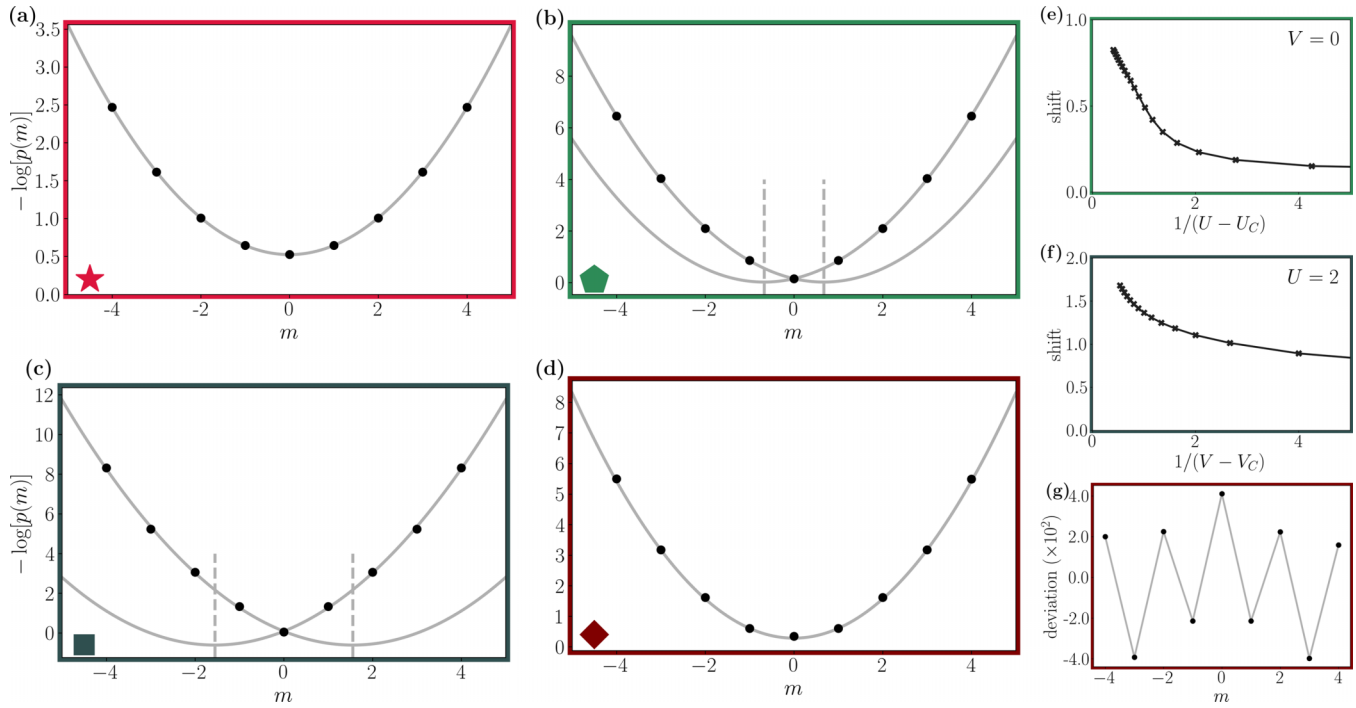

FIG. 3. The logarithm of the PDF (black points) is plotted for a representative configuration of the (a) SF phase [red star; $(U, V) = (0.5, 0.5)$], (b) MI phase [green pentagon; $(U, V) = (5.5, 0.5)$], (c) CDW phase [gray square; $(U, V) = (2, 4.5)$], and (d) HI phase [brown diamond; $(U, V) = (5, 3.3)$]. The gray lines show the fit of the PDF in terms of Gaussian envelopes and their shifts, as discussed in the main text. For both MI and CDW, the behavior is linear for small $|m|$, in compliance with horizontally shifted parabolas: on the right we show the shift of parabolas' minima from $m = 0$ as a function of the inverse distance from the critical point for MI (e) and CDW (f). It is apparent that they tend, respectively, to 1 and 2 deep in the phases, as predicted by perturbation theory in the text. For the HI, the dominant feature is a vertical shift between parabolas for the different parities of m: (g) shows a magnification thereof.

can be exploited to distinguish such gapped phases from all the others. We verified that the values of the α coefficient of the fit $-\ln[p(m)] = \alpha|m| + \beta m^2 + \gamma$ is nonzero only in the MI and CDW. The change rate of the coefficient along the phase transitions manifests again their nature [41]. We also stress that for the single boundary partition of some specific models, instead, the PDF may assume asymmetric shapes; see a description for the XXZ open chain in [6].

Finally, a direct inspection of the PDF in the HI phase reveals the typical footprint of the topological order. A detailed description can be obtained by truncating the maximum site occupation to $n_{\max} = 2$ bosons and mapping the EBH model to a spin-1 Heisenberg model [37,45,46]. In this framework the configurations of the HI appear as a *dilute antiferromagnet* of doblons (2) and holons (0) separated by an undetermined number of single occupations (1), $|\ldots 21\ldots 10\ldots 21\ldots 10\ldots\rangle$ [46]. Noticeably, the PDF of this topologically gapped phase, panel 3(d), resembles very closely the Gaussian PDF of the gapless phase, with the only signature of a slight shift for even/odd Gaussians [see Fig. 3(g)], alluding to the underlying parity-string order parameter. This explains the sensibly reduced, though still sizable, residuals in Fig. 1.

V. CONCLUSIONS

In conclusion, we have shown that the probability density function of the occupation number of a portion of the system (and simple fits thereof) can be a powerful agnostic inspection tool for the phase diagram of quantum many-body systems. For the extended Bose-Hubbard model, the obtained results are comparable with much more sophisticated analysis both via traditional methods dealing with gap scalings and correlation functions [36] and via modern machine learning approaches fed with the ES [15]. We claim that the PDF provides the best intermediate quantity between the whole ES and the bipartite number fluctuations [3] also for automatic detection protocols, since it combines the advantage of being easily accessible in modern experiments (e.g., quantum gas microscopes) with the wealth of information about the full many-body state, while requiring little prior knowledge about the emerging phases. Moreover, we foresee the method to be valid more in general: An extension beyond zero-temperature regimes and one-dimensional systems will be an appealing follow-up of this work.

ACKNOWLEDGMENTS

We acknowledge support from the Deutsche Forschungsgemeinschaft (DFG), Grant No. 277101999, within the CRC network TR 183 (subproject B01); the Alexander von Humboldt Foundation; the Provincia Autonoma di Trento, from Q@TN (the joint laboratory between University of Trento, FBK-Fondazione Bruno Kessler, INFN-National Institute for Nuclear Physics, and CNR-National Research Council);

and from the Italian MIUR under the PRIN2017 project CEnTraL. We gratefully acknowledge discussions with M. Kiefer-Emmanouilidis and A. Haller. The authors gratefully acknowledge the Gauss Centre for Supercomputing e.V. [47] for funding this project by providing computing time through the John von Neumann Institute for Computing (NIC) on the GCS Supercomputer JUWELS (Grant NeTeNeSyQuMa) and JURECA (institute project PGI-8) at Jülich Supercomputing Centre (JSC). The MPS simulations were run with a code based on a flexible Abelian symmetric tensor networks library, developed in collaboration with the group of S. Montangero (Padua).

[1] G. Vidal, J. I. Latorre, E. Rico, and A. Kitaev, Entanglement in Quantum Critical Phenomena, Phys. Rev. Lett. **90**, 227902 (2003).

[2] P. Calabrese and J. Cardy, Entanglement entropy and quantum field theory, J. Stat. Mech.: Theory Exp. (2004) P06002.

[3] H. F. Song, S. Rachel, and K. Le Hur, General relation between entanglement and fluctuations in one dimension, Phys. Rev. B **82**, 012405 (2010).

[4] P. Calabrese and A. Lefevre, Entanglement spectrum in one-dimensional systems, Phys. Rev. A **78**, 032329 (2008).

[5] A. M. Läuchli, Operator content of real-space entanglement spectra at conformal critical points, arXiv:1303.0741

[6] V. Alba, M. Haque, and A. M. Läuchli, Boundary-Locality and Perturbative Structure of Entanglement Spectra in Gapped Systems, Phys. Rev. Lett. **108**, 227201 (2012).

[7] H. Li and F. D. M. Haldane, Entanglement Spectrum as a Generalization of Entanglement Entropy: Identification of Topological Order in Non-Abelian Fractional Quantum Hall Effect States, Phys. Rev. Lett. **101**, 010504 (2008).

[8] F. Pollmann, A. M. Turner, E. Berg, and M. Oshikawa, Entanglement spectrum of a topological phase in one dimension, Phys. Rev. B **81**, 064439 (2010).

[9] A. Chandran, M. Hermanns, N. Regnault, and B. A. Bernevig, Bulk-edge correspondence in entanglement spectra, Phys. Rev. B **84**, 205136 (2011).

[10] X.-G. Wen, *Quantum Field Theory of Many-Body Systems From the Origin of Sound to an Origin of Light and Electrons* (Oxford Graduate Texts, Oxford, 2007).

[11] B. Zeng, X. Chen, D.-L. Zhou, and X.-G. Wen, *Quantum Information Meets Quantum Matter* (Springer, New York, 2019).

[12] X. Deng and L. Santos, Entanglement spectrum of one-dimensional extended Bose-Hubbard models, Phys. Rev. B **84**, 085138 (2011).

[13] L. Lepori, G. De Chiara, and A. Sanpera, Scaling of the entanglement spectrum near quantum phase transitions, Phys. Rev. B **87**, 235107 (2013).

[14] E. P. Van Nieuwenburg, Y. H. Liu, and S. D. Huber, Learning phase transitions by confusion, Nat. Phys. **13**, 435 (2017).

[15] K. Kottmann, P. Huembeli, M. Lewenstein, and A. Acín, Unsupervised Phase Discovery with Deep Anomaly Detection, Phys. Rev. Lett. **125**, 170603 (2020).

[16] D. Contessi, E. Ricci, A. Recati, and M. Rizzi, Detection of Berezinskii-Kosterlitz-Thouless transition via generative adversarial networks, SciPost Phys. **12**, 107 (2022).

[17] A. Nahum, J. Ruhman, S. Vijay, and J. Haah, Quantum Entanglement Growth under Random Unitary Dynamics, Phys. Rev. X **7**, 031016 (2017).

[18] B. Skinner, J. Ruhman, and A. Nahum, Measurement-Induced Phase Transitions in the Dynamics of Entanglement, Phys. Rev. X **9**, 031009 (2019).

[19] Y. Li, X. Chen, and M. P. A. Fisher, Measurement-driven entanglement transition in hybrid quantum circuits, Phys. Rev. B **100**, 134306 (2019).

[20] A. J. Daley, H. Pichler, J. Schachenmayer, and P. Zoller, Measuring Entanglement Growth in Quench Dynamics of Bosons in an Optical Lattice, Phys. Rev. Lett. **109**, 020505 (2012).

[21] R. Islam, R. Ma, P. M. Preiss, M. Eric Tai, A. Lukin, M. Rispoli, and M. Greiner, Measuring entanglement entropy in a quantum many-body system, Nature (London) **528**, 77 (2015).

[22] A. M. Kaufman, M. E. Tai, A. Lukin, M. Rispoli, R. Schittko, P. M. Preiss, and M. Greiner, Quantum thermalization through entanglement in an isolated many-body system, Science **353**, 794 (2016).

[23] T. Brydges, A. Elben, P. Jurcevic, B. Vermersch, C. Maier, B. P. Lanyon, P. Zoller, R. Blatt, and C. F. Roos, Probing Rényi entanglement entropy via randomized measurements, Science **364**, 260 (2019).

[24] G. Giudici, T. Mendes-Santos, P. Calabrese, and M. Dalmonte, Entanglement Hamiltonians of lattice models via the Bisognano-Wichmann theorem, Phys. Rev. B **98**, 134403 (2018).

[25] Z. Ma, C. Han, Y. Meir, and E. Sela, Symmetric inseparability and number entanglement in charge-conserving mixed states, Phys. Rev. A **105**, 042416 (2022).

[26] A. Lukin, M. Rispoli, R. Schittko, M. E. Tai, A. M. Kaufman, S. Choi, V. Khemani, J. Léonard, and M. Greiner, Probing entanglement in a many-body-localized system, Science **364**, 256 (2019).

[27] M. Kiefer-Emmanouilidis, R. Unanyan, M. Fleischhauer, and J. Sirker, Evidence for Unbounded Growth of the Number Entropy in Many-Body Localized Phases, Phys. Rev. Lett. **124**, 243601 (2020).

[28] M. Kiefer-Emmanouilidis, R. Unanyan, M. Fleischhauer, and J. Sirker, Unlimited growth of particle fluctuations in many-body localized phases, Ann. Phys. **435**, 168481 (2021), special issue on localization 2020.

[29] H. F. Song, S. Rachel, C. Flindt, I. Klich, N. Laflorencie, and K. Le Hur, Bipartite fluctuations as a probe of many-body entanglement, Phys. Rev. B **85**, 035409 (2012).

[30] S. Rachel, N. Laflorencie, H. F. Song, and K. Le Hur, Detecting Quantum Critical Points Using Bipartite Fluctuations, Phys. Rev. Lett. **108**, 116401 (2012).

[31] I. Klich and L. Levitov, Quantum Noise as an Entanglement Meter, Phys. Rev. Lett. **102**, 100502 (2009).

[32] M. Goldstein and E. Sela, Symmetry-Resolved Entanglement in Many-Body Systems, Phys. Rev. Lett. **120**, 200602 (2018).

[33] R. Bonsignori, P. Ruggiero, and P. Calabrese, Symmetry resolved entanglement in free fermionic systems, J. Phys. A: Math. Theor. **52**, 475302 (2019).

[34] L. Capizzi, P. Ruggiero, and P. Calabrese, Symmetry resolved entanglement entropy of excited states in a CFT, J. Stat. Mech.: Theory Exp. (2020) 073101.

[35] P. Calabrese, M. Collura, G. D. Giulio, and S. Murciano, Full counting statistics in the gapped XXZ spin chain, Europhys. Lett. **129**, 60007 (2020).

[36] D. Rossini and R. Fazio, Phase diagram of the extended Bose–Hubbard model, New J. Phys. **14**, 065012 (2012).

[37] S. Ejima, F. Lange, and H. Fehske, Spectral and Entanglement Properties of the Bosonic Haldane Insulator, Phys. Rev. Lett. **113**, 020401 (2014).

[38] K. Kottmann, A. Haller, A. Acín, G. E. Astrakharchik, and M. Lewenstein, Supersolid-superfluid phase separation in the extended Bose-Hubbard model, Phys. Rev. B **104**, 174514 (2021).

[39] D. Contessi, D. Romito, M. Rizzi, and A. Recati, Collisionless drag for a one-dimensional two-component Bose-Hubbard model, Phys. Rev. Res. **3**, L022017 (2021).

[40] N. Laflorencie and S. Rachel, Spin-resolved entanglement spectroscopy of critical spin chains and Luttinger liquids, J. Stat. Mech.: Theory Exp. (2014) P11013.

[41] See Supplemental Material at http://link.aps.org/supplemental/10.1103/PhysRevB.107.L121403 for additional details.

[42] T. D. Kühner, S. R. White, and H. Monien, One-dimensional Bose-Hubbard model with nearest-neighbor interaction, Phys. Rev. B **61**, 12474 (2000).

[43] T. Giamarchi, *Quantum Physics in One Dimension* (Oxford University Press, New York, 2003).

[44] M. Gerster, M. Rizzi, F. Tschirsich, P. Silvi, R. Fazio, and S. Montangero, Superfluid density and quasi-long-range order in the one-dimensional disordered Bose-Hubbard model, New J. Phys. **18**, 015015 (2016).

[45] W. Chen, K. Hida, and B. C. Sanctuary, Ground-state phase diagram of $s = 1$XXZ chains with uniaxial single-ion-type anisotropy, Phys. Rev. B **67**, 104401 (2003).

[46] E. Berg, E. G. Dalla Torre, T. Giamarchi, and E. Altman, Rise and fall of hidden string order of lattice bosons, Phys. Rev. B **77**, 245119 (2008).

[47] www.gauss-centre.eu.